Coarsening effects on the liquid permeability in foam-filled porous media

Margaux Ceccaldi, Vincent Langlois, and Olivier Pitois [*]
Université Gustave Eiffel, Ecole des Ponts et Chaussées, CNRS, Laboratoire Navier, F-77454 Marne-la-Vallée, France

Marielle Guéguen
Université Gustave Eiffel, MAST-CPDM, F-77454 Marne-la-Vallée, France

Daniel Grande [†]
Université Paris Est Creteil, CNRS, Institut de Chimie et des Matériaux Paris-Est (ICMPE), 2 rue Henri Dunant, 94320 Thiais, France

S. Vincent-Bonnieu
European Space Agency, Keplerlaan 1, 2200 AG Noordwijk, The Netherlands

(Received 15 May 2024; accepted 2 July 2024; published 23 July 2024)

Injection of liquid foam through soils is increasingly used in applications such as soil remediation or soil improvement, where it is also crucial to control the liquid relative permeability through the foam-filled soil. We have measured the time dependence of the liquid permeability of granular packings initially filled with liquid foam for different values of the liquid saturation. It is shown that, systematically, permeability increases significantly over time before reaching saturation. We have demonstrated that this evolution is directly related to the coarsening of the liquid foam confined in the pore space. We have shown how the evolution of the liquid permeability can be predicted from the knowledge of the bubble size evolution.

DOI: 10.1103/PhysRevFluids.9.074003

I. INTRODUCTION

Foam properties are particularly well suited for environmental remediation. The use of foam has emerged as a viable alternative to conventional flushing techniques for effectively extracting nonaqueous phase liquids from aquifers [1,2]. The entrapment of gas within bubbles enhances the stability of displacement processes in porous materials, thereby providing better control of remediation processes within reservoirs or aquifers [3], i.e., underground layers of permeable rock, sediment, or soil that contain groundwater. Additionally, foam can act as a barrier, reducing liquid permeability in porous substrates [4,5], thereby aiding in containing sources of contamination. In the realm of soil treatment, other specific applications of foam exist, such as in earth pressure balance tunneling in coarse-grained soils. When shield machines used to excavate tunnels (while providing support to prevent collapses) operate in sandy soils below the water level, water spewing frequently occurs, affecting the stability of the excavation face [6]. Foam is commonly injected into the soil chamber to reduce the permeability of excavated soils [6,7], thus mitigating the instability issue.

[*]Contact author: Olivier.Pitois@univ-eiffel.fr
[†]Present adress: Université de Strasbourg, CNRS, Institut Charles Sadron–UPR22, 23 rue du Loess, BP 84047, 67034 Strasbourg Cedex 2, France.

For all these applications, it is relevant to consider the water relative permeability of the foam-filled medium, defined by the ratio of the liquid permeability of the foam-filled porous medium at liquid saturation S_w, $k_D(S_w)$, and the liquid permeability of the same medium as it is fully saturated with liquid, $k_D(S_w = 1)$:

$$k_{\text{rel}} = \frac{k_D(S_w)}{k_D(S_w = 1)}. \tag{1}$$

This crucial parameter has been studied since the 1960s: Bernard *et al.* [8] have demonstrated that the relative permeability of the medium is affected by the presence of foam in the porosity to a comparable extent as the nonfoamed air phase at the same volume fraction. Subsequently, other researchers have explored this effect. It has been observed that the relative permeability decreases by a factor of 10^3 –10^4 when foam introduction reduces liquid saturation to values below 0.2 [9,10].

On a theoretical level, this issue involving flows in triphasic systems presents serious challenges in terms of modeling. However, since its inception, the analysis of permeability results has been mainly based on that of unsaturated porous media permeability. This remains the case, as evidenced by recent publications on the subject [9–11]. This analysis relies on correlations between hydraulic permeability measurements and liquid saturation as a function of capillary pressure in the medium. Numerous analytical curves have been proposed to describe these correlations, with the Van Genuchten and Brooks-Corey curves being among the most well known [12]. On the other hand, a few alternative approaches have recently emerged. For instance, Wang *et al.* [13] aimed to explicitly describe the permeability of confined liquid foam within the porous space of grain packings. The expression for the permeability of the medium depends explicitly on the bubble/grain size ratio, i.e., $r = D_b/D_g$, but the experimental data collected by the authors did not allow for a quantitative investigation of this parameter. Investigating the effect of this ratio was the main objective of a recent study, and in agreement with the theoretical expression proposed by Wang *et al.* [13], it appears that the relative water permeability of foam-filled granular packings expresses as [14]

$$k_{\text{rel}} = \alpha(\phi_p) \times r^2 f(r) \times \widetilde{k}_{f0}(S_w), \tag{2}$$

where $\alpha(\phi_p) = 180(1 - \phi_p)^2/\phi_p^2$ is a constant fixed by the pore volume fraction ϕ_p of the granular packing, $\widetilde{k}_{f0}(S_w)$ is the dimensionless liquid permeability of the bulk foam, and $f(r)$ accounts for the confinement effects. In the study we herein proposed, we continue the work that led to Eq. (2), and we attempt to incorporate other effects that have been overlooked up to now. In particular, the intrinsic aging of the foam confined within the porosity of the medium is completely absent from previous studies. Coarsening, for example, is an inherent phenomenon in the general behavior of liquid foam: under the combined effects of gas pressure differences between bubbles and gas solubility in the liquid, gas exchanges occur between bubbles, thus leading to a decrease in the number of bubbles present and an increase in the average size of these bubbles [15]. This phenomenon has been the subject of numerous studies in the past, and very recently, the coarsening of foams has been studied aboard the International Space Station, providing very useful information about coarsening kinetics and bubble size distribution over a wide range of liquid volume fractions [16,17]. In the case of foams with liquid fractions as high as 35%, the steady-state (or self-similar) regime of coarsening is marked by a progressive increase in the average bubble diameter over time, whereby

$$D_b(t) = \left[D_b^2(t_0) + \Omega(t - t_0)\right]^{1/2}, \tag{3}$$

where Ω is the coarsening rate and t_0 is the time corresponding to the start of the steady state [15,18]. It is noteworthy that the coarsening process is impacted by pore confinement. It has been observed that when the average bubble size is much smaller than the boundary, the coarsening process seems to behave similarly to bulk foam. However, as bubbles approach the size of the geometric confinement, they begin to experience confinement effects, leading to a decrease in the coarsening rate [19]. Notably, when properly confined, a polydisperse distribution of gas bubbles exhibits an *anticoarsening* phenomenon, wherein larger bubbles diffuse into smaller ones, ultimately resulting

in a monodisperse distribution [20–23] where each pore is filled with one bubble. It is noteworthy that the two-dimensional (2D) geometries selected for visualizing the previously reported bubble growth do not enable a quantitative comparison with the three-dimensional (3D) reference case herein investigated.

With recent clarification on the impact of the bubble/grain size ratio, it is foreseeable that in the presence of coarsening, the permeability of porous media filled with foam will vary over time, and, indeed, we cannot exclude that some of the permeability results we have previously reported may have been affected by this effect. Specifically, one can anticipate a coupling between the liquid flow through the medium and the coarsening process of the confined foam. The question that arises is as follows: Can we describe this evolution with the elements currently available to us, i.e., Eqs. (2) and (3)? With the aim of addressing this question, we conducted a series of experiments to measure both the permeability of such systems over time and the size of the bubbles observed at the sample wall under investigation.

II. MATERIALS AND METHODS

Anionic surfactants such as sodium alpha olefin sulfonate, sodium laureth sulfate, or dihexyl sulfosuccinate are often used for remediation purposes [10]. Here we have chosen to use an aqueous solution of a commercial alkyl polyglucoside (Glucopon 225DK from BASF, purity 70%, CMC 2 g/l), a nonionic surfactant dosed at 10 g/l in water. Alkyl polyglucosides are biodegradable surfactants derived from natural raw materials, typically glucose (from corn starch) and fatty alcohols (derived from coconut or palm kernel oil). Previous experiments with Glucopon showed their ability to produce very stable foams in porous media [14].

The porous medium was made by piling monodisperse grains (glass beads) in a glass column. Grains diameter D_g is equal to 2 or 1 mm with $\Delta D_g/D_g \approx 8\%$–$10\%$. We determined the porosity of the medium as $\phi_p = 1 - V_g/V_{\text{pack}}$. The volume of the grains V_g is determined from the ratio of their mass m_g to the density of the solid grains ρ_g. The latter parameter was measured by the liquid displacement method: a mass m_g of grains was immersed into a volume of water V_e and the resulting total volume V_t, i.e., water+grains, was measured: $\rho_g = m_g/(V_t - V_e)$. For each experiment, the mass of grains used to prepare the packing was weighted before filling the column with the grains. A grid was added to the bottom of the column so that the grains were retained in the column while allowing the foam to pass without breaking the bubbles. After filling the column with the grains, the height H of the packing was measured and its volume V_{pack} was determined from the cross section $S = 527\ \text{mm}^2$ of the column. The porosity was then calculated by the relation $\phi_p = 1 - m_g/(\rho_g V_{\text{pack}})$. For both 2 and 1 mm grains we found $\phi_p = 0.38$, which is in the expected range.

The setup we used permits one to control liquid foams in terms of bubble size (monodisperse) and liquid volume fraction: a flow of nitrogen was pushed to one inlet of a small T junction, while a flow of foaming solution was pushed to the other inlet, producing bubbles at the outlet. The resulting bubbles were collected in a vertical glass column where a camera placed at the wall of the column allowed one to measure their size thanks to prior calibration. Here we produced bubbles with diameter $D_b = 500\ \mu\text{m}$ with $\Delta D_b/D_b \leqslant \pm 3\%$. As explained in detail elsewhere [14], we are able to control both the bubble size and the liquid volume fraction S_w of the produced foam. Prior to experiment with the grain packings, the intrinsic liquid permeability k_{f0} of the monodisperse foam was measured thanks to the so-called *forced drainage method* (see [14] for more details). The results are well described by the following expression:

$$\tilde{k}_{f0}(S_w) = \frac{k_{f0}(S_w)}{D_b^2} = \frac{S_w^{3/2}}{\beta_0\left(1 - 2.7S_w + 2.2S_w^2\right)^2} \tag{4}$$

with $\beta_0 = 1250$. This equation characterizes fully the hydraulic behavior of the unconfined monodisperse bulk foam.

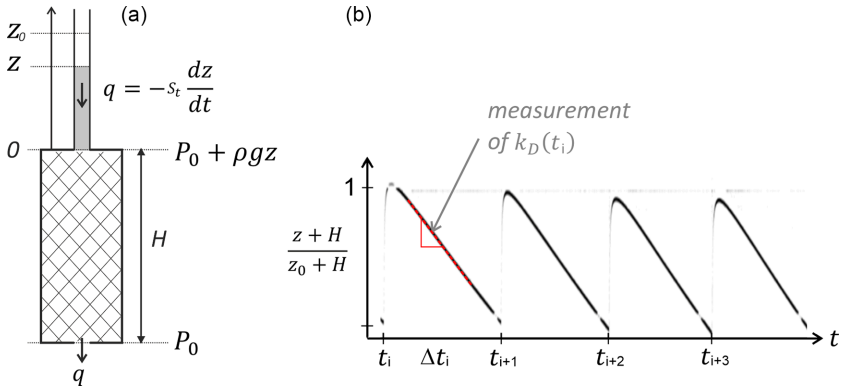

FIG. 1. Falling head permeability method. (a) The liquid height is measured in the tube at the top of the granular/foam column which allows the liquid flow through the column to be determined, in the situation where the bubbles are not carried away by the flow. Liquid is introduced again after a duration $\Delta t \approx 150$–300 s. This make the liquid height change abruptly in the tube [see (b)]. (b). Variation of the liquid height in the tube at the top of the sample column. For each decrease of the liquid height, the slope allows of the Darcy liquid permeability to be determined.

The produced foam was allowed to flow through the porous column. We monitored the foam at the exit of the column until we found the monodisperse foam introduced, proving that there was no film breakage. Therefore, at that stage, the size (volume) of the bubbles inside the bead packing is that prepared in the foaming column. In addition, weighings of the filled column confirmed that the volume fraction of liquid contained in the porosity of the medium matched the targeted S_w value within the measurement error range, i.e., $\Delta S_w/S_w \leqslant \pm 20\%$. Therefore, at this stage, the grain packing is filled with bubbles of size $D_b = 500$ µm and the liquid saturation is S_w.

In order to measure the permeability of our samples as a function of time, we adapted the so-called *falling head permeability method* [24]. The height H of the granular column was chosen to be equal to 64 mm in order to decrease the duration of the experiment. Then a tube was placed above the column, as shown in Fig. 1, and a volume v_t of surfactant solution was introduced into the tube using a syringe pump. The pressure imposed by the height z of the liquid in the tube allows the liquid to flow into the foam, through the granular packing. The kinetics of this flow was followed by measuring z as a function of time. In this configuration, the liquid flow rate q entering the packing depended on the cross-sectional area s_t of the tube and the variation of height z with time: $q = -s_t dz/dt$. Darcy's law allows us to relate the flow rate q of the liquid to the permeability k_D of the medium, i.e., the permeability of the grains plus bubbles, assuming that, in agreement with our observations, only the liquid is flowing:

$$-\frac{s_t}{S}\frac{dz}{dt} = \frac{k_D}{\eta}\frac{\rho g(z+H)}{H}. \tag{5}$$

The resolution of this equation provides the temporal evolution of the altitude z as a function of the permeability k_D:

$$\frac{z+H}{z_0+H} = \exp\left(-\frac{S}{s_t}\frac{k_D}{\eta}\frac{\rho g}{H}t\right). \tag{6}$$

Such a measurement was performed every $\Delta t \approx 150$–300 s, which allowed one to get the k_D values as a function of time. Typical examples are shown in Fig. 1. In the following, the relative liquid permeability is calculated as $k_{\rm rel} = k_D(S_w)/k_{\rm CK}$, where $k_{\rm CK} = \phi_p^3 D_g^2/180(1-\phi_p)^2$ is the *Carman-Kozeny* expression [25,26].

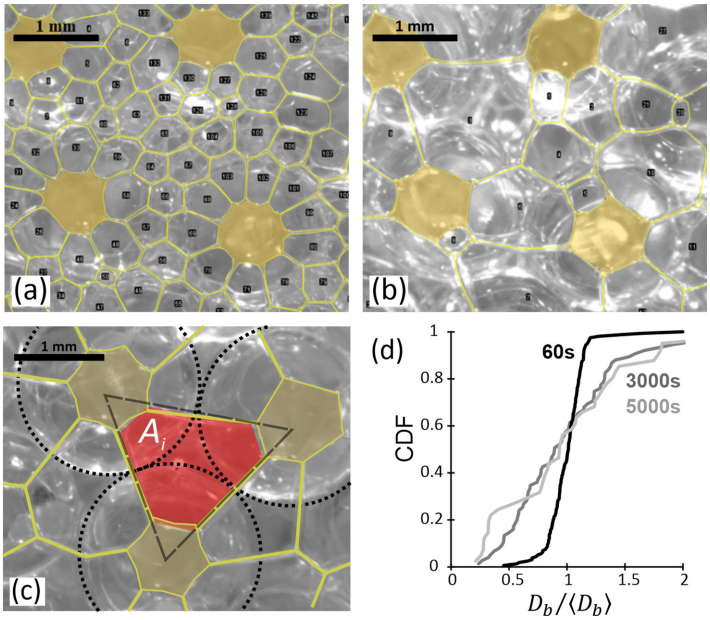

FIG. 2. Foam bubbles as seen at the wall. (a) and (b) For the sake of clarity the outline of the area covered by each bubble is highlighted, and the area covered by the liquid bridges, around the contact points between the grains and the wall, is colored. (c) Area A_i covered at the wall by a large bubble in a pore formed between three grains at the wall. The outline of the grains is highlighted by dotted circles. The area A_i corresponds to approximately 80% of the area of the triangle, whose vertices are positioned where the grains come into contact with the wall. (d) Typical cumulative distribution function of bubble diameters divided by the average bubble size obtained from size measurements at the wall, for several times: 60, 3000, and 5000 s.

In order to determine the bubble size, we used images of the column wall (see Fig. 2). We identified a reference area A_T at the wall from which the area of the liquid bridges was subtracted and we counted the number N of bubbles it contained. The average bubble diameter was estimated as follows:

$$\langle D_b\rangle = \xi\left(\frac{4A_T}{\pi N}\right)^{1/2}, \tag{7}$$

where $\xi = 0.9$ is a calibration coefficient accounting for the bubble shape at the wall. This coefficient was determined by comparing the initial bubble size, which was determined independently before the foam production step, i.e., $D_b = 500$ μm, with $(4A_T/\pi N)^{1/2}$. Because bubbles grow, this coefficient may change in the same time. In order to estimate this possible variation, we consider the typical bubble configuration that we often observe at the end of the coarsening process [see Fig. 2(c)]. The area covered by the bubble at the wall is $A_i \approx 0.8\times\frac{\sqrt{3}}{4}D_g^2$, so the bubble diameter deduced from the surface is $D_b^{(A_i)} = (\frac{4A_i}{\pi})^{1/2} \approx (0.8\times\frac{\sqrt{3}}{\pi})^{1/2}D_g \approx 0.66D_g$. Now we consider the true volume of the bubble occupying the pore: $V_i \approx (\sqrt{3}-\frac{\pi}{3})\frac{D_g^3}{8}$, so the bubble diameter deduced from this volume is $D_b^{(V_i)} = [\frac{3}{4\pi}(\sqrt{3}-\frac{\pi}{3})]^{1/3}D_g \approx 0.55D_g$. The coefficient we are looking for is $\xi = D_b^{(V_i)}/D_b^{(A_i)} \approx 0.82$. This value, which accounts for the bubble shape in the final configuration (coarsened configuration), is not so different from that determined experimentally in the initial configuration, therefore we will always use the same value thereafter, i.e., $\xi = 0.9$. It is noteworthy that in this paper the average bubble size $\langle D_b(t)\rangle$ is simply denoted $D_b(t)$.

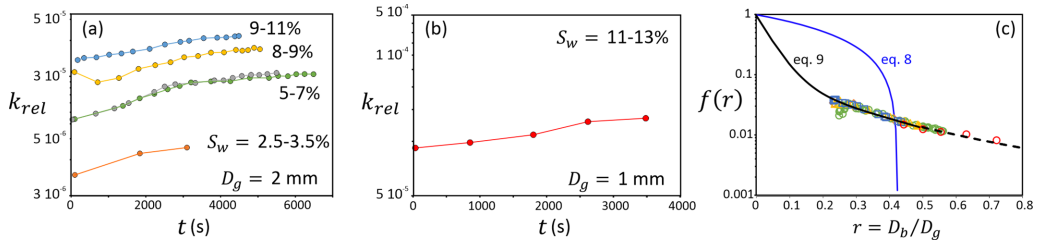

FIG. 3. (a) Liquid relative permeability measured for foam-filled granular packings as a function of time for 2 mm grains and for several values of the liquid saturation S_w as indicated. (b) Liquid relative permeability measured as a function of time for 1 mm grains and liquid saturation S_w as indicated. (c) Solid lines correspond to $f(r)$ functions given by Eqs. (8) and (9) for $r \leqslant 0.5$. For $r > 0.5$ the dotted line is a guide for the eye. Symbols represent the data of figures (a) and (b). Note that the parameter S_w was allowed to vary within the range indicated in order to bring the experimental points as close as possible to the curves $f(r)$. We used $S_w = 0.03$ (orange symbols), 0.058 (green), 0.062 (gray), 0.082 (yellow), 0.098 (blue), and 0.12 (red).

III. RESULTS AND DISCUSSION

In the following section, we present our results for both the liquid relative permeability of the foam-filled samples and the bubble size as a function of time. The results for both 2- and 1-mm grain packings are presented in Figs. 3(a) and 3(b) for several liquid saturations S_w. We stress that the initial bubble size $D_b(0)$ is equal to 500 μm for all the samples. As a first comment, the measured relative permeabilities are within the range 5×10^{-6} to 5×10^{-5}, which is two orders of magnitude smaller than previously reported values, e.g., [9,11,27]. This is due to the fact that we are studying systems containing much more gas phase than previous studies, with liquid saturation as low as 0.03. It is shown that whatever the grain size and liquid saturation, liquid relative permeability $k_{\mathrm{rel}}(t)$ always increases in the same way as a function of time: a significant increase followed by a much more moderate increase or a plateau. The characteristic duration for such an evolution is on the order of 1 h. Therefore, foam-filled porous media exhibit aging at constant liquid saturation.

The time evolutions for the bubble sizes measured at the wall of the column are presented in Figs. 4(a)–4(e). The bubbles are shown to grow as a function of time, starting from initial monodisperse size $D_b(0) \approx 0.5$ mm and reaching up to $D_b(t) \approx 1.3$ mm for the 2 mm grains. We recall that bubble coarsening in model quasi-2D porous media [22,23] have revealed the so-called anticoarsening phenomenon, where bubbles stop coarsening as their size reaches the pore size. This is precisely what we observe at the wall of our 3D samples: coarsening stops when each pore is filled with one bubble. By considering such a final bubble configuration at the wall [see Fig. 2(c)], the bubble diameter is $D_b \approx 0.6 D_g$. Therefore, we do not expect to observe a stop in coarsening for reported D_b values significantly smaller than ≈0.6 mm for the 1 mm grains, and ≈1.2 mm for the 2 mm grains. This is consistent with the data shown in Fig. 4, bearing in mind that some bubbles can occupy double pores, for example.

It is clear that the characteristic time over which bubble growth occurs is comparable to that describing the permeability increase reported in the previous paragraph, which indicated that both phenomena are intimately related. Our main objective is to quantitatively explain the increase in permeability measured over time for the foam-filled samples in relation with the coarsening process. First of all we compare the coarsening rate Ω [see Eq. (3)] of the foam confined in the pore space with values available for bulk foam in the literature. Ω depends on the liquid-gas surface tension, the gas diffusion coefficient in the liquid, the Henry solubility coefficient of the gas in the liquid, the gas molar volume, the foam liquid fraction and the foam film thickness. Our data seem to be compatible with Eq. (3) for times t larger than $t_0 \approx 2000$ s for all the samples. This time is expected to be related to the initial (transitional) regime that characterizes initial monodisperse bubble size distributions and which must be completed before entering the coarsening regime described above [15]. This can

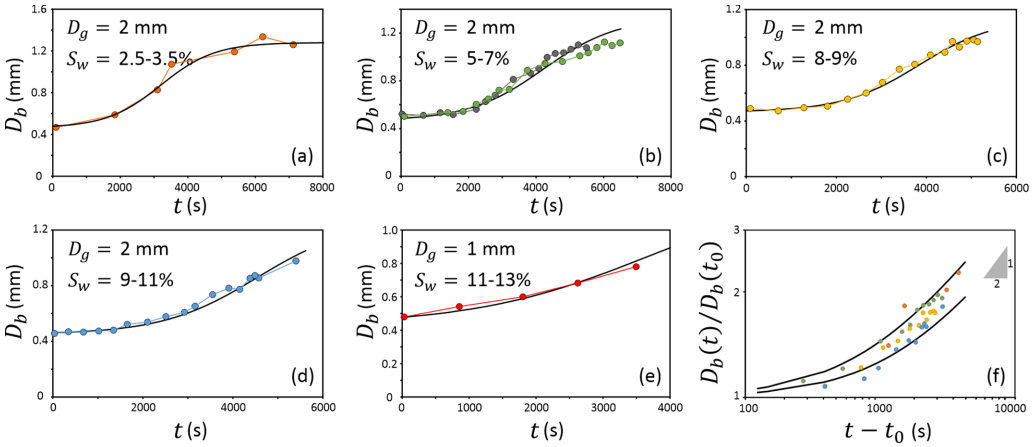

FIG. 4. Bubble sizes measured at the wall of our sample column as a function of time (sample age). (a)–(d): 2 mm grains and several values of the liquid saturation as indicated. Solid lines are sigmoidal functions (see main text for more details) with parameters given in Table I. (e) 1 mm grains. Solid line is a sigmoidal function (see main text for more details) with parameters given in Table I. (f) Ratio of bubble size at age t and at age $t_0 \approx 2000$ s as a function of $(t - t_0)$ in log-log scales for all the samples (symbols). The gray triangle indicates the slope $1/2$ in the log-log scale. The solid lines correspond to Eq. (3) with $\Omega = 150$ μm^2/s (lower curve) and $\Omega = 250$ μm^2/s (upper curve).

be seen clearly in Fig. 2(d): consider the strong change in bubble size distribution between times 60 and 3000 s, while the distribution remains unchanged for longer times, except near the coarsening arrest (not shown here). Therefore, we plot Eq. (3) against our data $D_b(t)/D_b(t_0)$ as a function of $t - t_0$ in Fig. 4(f). It is noteworthy that Eq. (3) is similar to a power law with exponent $1/2$ for $(t - t_0) \gg D_b^2(t_0)/\Omega$. As shown in Fig. 4(f), this condition cannot be reached before coarsening stops due to geometrical interactions of the bubbles in the pore space. However, the bubble growth can be reasonably described by Eq. (3) taking coarsening rates Ω within the range 150–250 μm^2/s, depending on the liquid fraction [see Fig. 4(f)]. This range of values is consistent with literature, although the differences in coarsening rate for the different values of liquid saturation may not be so marked as expected: for example, a factor 2.4 is expected between coarsening rates at 12% and 3% [16] of liquid. It is difficult to say more in the current state; literature currently provides too little quantitative information about foam coarsening rates within confined spaces [19]. A specific and more comprehensive study on foam coarsening in porous media may perhaps provide more insights. However, this study is outside the scope of our work on permeability.

For now, we will try to use the results for the observed bubble growth to account for the increase in the liquid permeability. We refer to Eq. (2), where the liquid relative permeability is related to the bubble-to-grain size ratio, r, to the intrinsic dimensionless foam permeability at liquid volume fraction S_w, $\widetilde{k}_{f0}(S_w)$, and the foam permeability reduction due to confinement in the pore space, described by the function $f(r)$. Herein, we refer to both the theoretical work of Wang *et al.* [13],

$$f(r) = 1 - \left(\frac{\pi}{2}\frac{1-\phi_p}{\phi_p}\right)r, \tag{8}$$

and the empirical function proposed elsewhere [14], which can be conveniently described by the following double exponential function:

$$f(r) = A\,\exp\left(\frac{-r}{a}\right) + B\,\exp\left(\frac{-r}{b}\right) \tag{9}$$

TABLE I. Parameters (s_1, s_2, s_3, and s_4) used in sigmoid functions to describe the bubble size time evolution presented in Fig. 4 for systems (a)–(e).

System	D_g (mm)	S_w (%)	s_1	s_2	s_3	s_4 (s)
(a)	2	2.5–3.5	0.96	1.7	4.0	800
(b)	2	5–7	0.95	1.8	3.8	1100
(c)	2	8–9	0.95	1.4	4.5	850
(d)	2	9–11	0.95	1.7	4.3	1050
(e)	1	11–13	0.92	1.7	2.8	1300

with $A = 0.92$, $a = 0.045$, $B = 0.08$, and $b = 0.28$. It is to say that the range of values for r is $r \leqslant 0.5$, whereas the range defined by Eq. (8) is $r \leqslant 0.4$.

In order to compare these functions $f(r)$ with our experimental results, we need to associate each permeability $k_{\mathrm{rel}}(t)$ value with the corresponding D_b value. To do this, it is convenient to have functions to describe the evolutions for $D_b(t)$. We have chosen to use sigmoidal functions of the form $D_b(t) = D_b(0)(s_1 + \frac{s_2}{1+\exp{(s_3 - \frac{t}{s_4})}})$, with parameters presented in Table I. Therefore, for each time t we determine the ratio $r = D_b(t)/D_g$ as well as the function $f(r) = k_{\mathrm{rel}}/\alpha r^2 \tilde{k}_{f0}$, according to Eq. (2). Corresponding values $f(r)$ are plotted in Fig. 3(c) with both Eqs. (8) and (9). It should be noted that the parameter S_w was allowed to vary within the range indicated in Fig. 3(c) in order to bring the experimental points as close as possible to the curves $f(r)$.

The comparison presented in Fig. 3(c) demonstrates agreement between our measurements and the empirical law, Eq. (9), determined previously for exclusively monodisperse systems. This indicates that considering the variation in average bubble size allows predicting induced permeability changes using Eqs. (2) and (9). However, the theoretical model by Wang *et al.,* Eq. (8), shows relatively significant disagreement. We do not have any evidence to explain where the observed disagreement arises. This suggests that modeling work is now needed to account for the evolution of $f(r)$ given by Eq. (9).

IV. CONCLUSION

We have measured as a function of time the liquid relative permeability of grain packings initially filled with liquid foam for different values of the liquid saturation. For all the samples the permeability is shown to increase as a function of time until a constant value is eventually observed, which highlights the significant aging of such systems. This increase corresponds typically to 60%–70% of the initial value. We demonstrate that this evolution is directly related to the coarsening of the liquid foam confined in the pore space. This shows that predicting the permeability of such systems also requires knowing the size of the bubbles confined at time t, not just those corresponding to the filling instant of the porous medium by the foam. Using the measured bubble size evolution combined with the intrinsic liquid permeability of the bulk foam, we have determined values corresponding to the function that describes the foam confinement effects as a function of the bubble-to-grain size ratio. These values were found to be very close to the empirical function proposed recently by Ceccaldi *et al.* [14] for monodisperse foam bubble distribution. On the other hand, current modeling of this function appears to be inappropriate and calls for further theoretical development.

ACKNOWLEDGMENTS

The authors gratefully acknowledge funding from the Labex MMCD provided by the national program Investments for the Future of the French National Research Agency (ANR-11-LABX-022), funding from the French National Research Agency (ANR-23-CE51-0030-01), and co-funding from the European Space Agency (reference I-2020-02017).

O.P., V.L., and M.C. contributed to the preparation of the experiment. M.C. did the measurements. O.P., V.L., and M.C. contributed to the analysis of the results. All the authors participated in the discussions and writing of the manuscript.

The authors declare no conflicts.

[1] S. Wang and C. Mulligan, An evaluation of surfactant foam technology in remediation of contaminated soil, Chemosphere **57**, 1079 (2004).

[2] O. Atteia, E. Estrada, and H. Bertin, Soil flushing: A review of the origin of efficiency variability, Rev. Environ. Sci. Bio/Technol. **12**, 379 (2013).

[3] G. J. Hirasaki, The steam-foam process, J. Pet. Technol. **41**, 449 (1989).

[4] H. Bertin, O. Apaydin, L. Castanier, and A. Kovscek, Foam flow in heterogeneous porous media: Effect of cross flow, SPE J. **4**, 75 (1999).

[5] A. Kovscek and H. Bertin, Foam mobility in heterogeneous porous media, Transp. Porous Media **52**, 17 (2003).

[6] L. Langmaack and K. F. Lee, Difficult ground conditions? Use the right chemicals! Chances–limits–requirements, Tunnelling Underground Space Technol. **57**, 112 (2016).

[7] X. Zhou and Y. Yang, Effect of foam parameters on cohesionless soil permeability and its application to prevent the water spewing, Appl. Sci. **10**, 1787 (2020).

[8] G. G. Bernard, L. W. Holm, and W. L. Jacobs, Effect of foam on trapped gas saturation and on permeability of porous media to water, Soc. Pet. Eng. J. **5**, 295 (1965).

[9] A. A. Eftekhari and R. Farajzadeh, Effect of foam on liquid phase mobility in porous media, Sci. Rep. **7**, 43870 (2017).

[10] C. Portois, C. S. Boeije, H. M. Bertin, and O. Atteia, Foam for environmental remediation: Generation and blocking effect, Transp. Porous Media **124**, 787 (2018).

[11] O. Atteia, H. Bertin, N. Fatin-Rouge, E. Fitzhenry, R. Martel, C. Portois, T. Robert, and A. Vicard, Application of foams as a remediation and blocking agent, in *Advances in the Characterisation and Remediation of Sites Contaminated with Petroleum Hydrocarbons. Environmental Contamination Remediation and Management*, 1st ed. (Springer, Cham, 2024), Chap. 17, pp. 591–622.

[12] A. Szymkiewicz, *Modelling Water Flow in Unsaturated Porous Media* (Springer, Berlin, Heidelberg, 2013).

[13] S. Wang, S. Huang, T. Qiu, J. Yang, J. Zhong, and Q. Hu, Analytical study of the permeability of a foam-conditioned soil, Int. J. Geomech. **20**, 06020019 (2020).

[14] M. Ceccaldi, V. Langlois, M. Guéguen, D. Grande, S. Vincent-Bonnieu, and O. Pitois, Liquid relative permeability through foam-filled porous media: Experiments, Phys. Rev. Fluids **8**, 024302 (2023).

[15] I. Cantat, S. Cohen-Addad, F. Elias, F. Graner, R. Höhler, O. Pitois, F. Rouyer, and A. Saint-Jalmes, *Foams: Structure and Dynamics* (Oxford University Press, Oxford, 2013).

[16] M. Pasquet, N. Galvani, A. Requier, S. Cohen-Addad, R. Höhler, O. Pitois, E. Rio, and A. Salonen, Coarsening transitions of wet liquid foams under microgravity conditions, Soft Matter **19**, 6267 (2023).

[17] N. Galvani, M. Pasquet, A. Mukherjee, A. Requier, S. Cohen-Addad, O. Pitois, R. Höhler, E. Rio, A. Salonen, D. J. Durian, and D. Langevin, Hierarchical bubble size distributions in coarsening wet liquid foams, Proc. Natl. Acad. Sci. USA **120**, e2306551120 (2023).

[18] O. Pitois, Foam ripening, in *Foam Engineering*, edited by P. Stevenson (Wiley-Blackwell, Chichester, 2012), Chap. 4, pp. 59–73.

[19] W. Yu and M. Kanj, Review of foam stability in porous media: The effect of coarsening, J. Pet. Sci. Eng. **208**, 109698 (2022).

[20] M. A. Forte, M. Rosa, and S. Findlay, Properties of peripheric cells in cellular structures, Philos. Mag. A **79**, 1853 (1999).

[21] M. Rosa and M. Fortes, Coarsening of two-dimensional foams confined by walls, Philos. Mag. A **79**, 1871 (1999).

[22] S. Jones, N. Getrouw, and S. Vincent-Bonnieu, Foam flow in a model porous medium: I. The effect of foam coarsening, Soft Matter **14**, 3490 (2018).
[23] K. Xu, R. Bonnecaze, and M. Balhoff, Egalitarianism among bubbles in porous media: An Ostwald ripening derived anticoarsening phenomenon, Phys. Rev. Lett. **119**, 264502 (2017).
[24] K. Terzaghi, R. B. Peck, and G. Mesri, *Soil Mechanics in Engineering Practice*, 3rd ed. (Wiley, New York, 1996).
[25] J. Kozeny, Ueber kapillare leitung des wassers im boden, Sitzungsber. Akad. Wiss. **136**, 271 (1927).
[26] P. Carman, Fluid flow through granular beds, Trans. Inst. Chem. Eng. London **15**, 150 (1937).
[27] P. Persoff, C. Radke, K. Pruess, S. Benson, and P. Witherspoon, A laboratory investigation of foam flow in sandstone at elevated pressure, SPE Reservoir Eng. **6**, 365 (1991).